Study of the Microstructure and Permeability of Building Stone Using X-ray Micro-tomography

Martin Vavro[1*], Kamil Souček[1], Leona Vavro[1], Lucie Georgiou[1], Jan Mrógala[1,2]

[1] Institute of Geonics, Czech Academy of Sciences, Studentská 1768/9, 708 00 Ostrava-Poruba, Czech Republic
[2] Department of Informatics and Computers, Faculty of Science, University of Ostrava, 30. dubna 22, 701 03 Ostrava, Czech Republic
* Corresponding author, e-mail: martin.vavro@ugn.cas.cz

Abstract
Fluid transport and storage properties of porous rocks are closely related to their microstructure. Porosity is one of the most important microstructural parameters due to its importance for transport of water, gases and dissolved salts, but also for mechanical, deformation and durability properties of geomaterials used in constructions. In this study, the X-ray computed micro-tomography (XCT) was used to study the spatial distribution of porosity and permeability within the Kocbeře sandstone, which represents a very well-known and long-term used building stone in the territory of the Czech Republic. The microstructure and composition of the Kocbeře sandstone were characterized by a complex of methods, including optical polarization microscopy, scanning electron microscopy coupled with energy dispersive spectroscopy, X-ray powder diffraction, X-ray fluorescence spectroscopy and mercury intrusion porosimetry (MIP). Values of porosity and permeability of the Kocbeře sandstone derived from XCT were compared with results of MIP as well as laboratory measurements of open porosity, hydraulic conductivity and gas permeability. A very good compliance was found between the average values of sandstone porosity determined by the XCT imaging analysis, MIP and experimentally determined open porosity. However, considerable heterogeneity of porosity in the individual analyzed subvolumes was detected using XCT. Very significant inhomogeneity was also found in the spatial distribution of permeability tensors calculated for individual subvolumes. The considerable dispersion of porosity and permeability values of sandstone at the microscale is given by its microstructure. The main role here is played by intense secondary silicification, which unevenly affects the clay matrix of the sandstone.

Keywords
building stone, pore microstructure, fluid permeability, anisotropy, X-ray computed micro-tomography

1 Introduction

Pore microstructure in porous media such as rocks and similar rock-like geomaterials involves size distribution, volume, shape, orientation and connectivity of pores and cracks and has a fundamental influence on many macroscopically observed properties such as rock strength and its deformation and fracture properties [1–4]. Together with related rock permeability, it is the crucial factor when assessing the suitability of the rock environment for such challenging engineering applications as gases storage, primarily CO_2, in geological formations or geological disposal of high-level radioactive waste [5–9]. While in the case of a deep geological repository of radioactive waste, it is necessary for the rock mass to have the lowest possible porosity and permeability, suitable CO_2 repositories, on the contrary, require a high degree of rock permeability due to a large amount of interconnected open pores and/or cracks. Pore network and connectivity of the pore space strongly affect fluid flow and solute transport in porous materials. Regardless of the natural or man-created, historical or today's origin, all the objects from porous materials are subjected to the corrosive environment causing its degradation. Action of moisture and dissolved ions present in the pore structure of material is a crucial deterioration process affecting its properties and behavior [10–12]. Porosity is therefore one of the main factors affecting the resistance of geomaterials such as rocks to weathering processes [13–15]. From this point of view, the study of porosity is of fundamental importance in the field of protection of building materials, rehabilitation of structures and heritage care [16].

Porosity is a scalar measure of void space in porous media and represents the ratio between void volume and total volume of the material. There are several types of

porosity [17], of which total porosity and open (effective) porosity are of fundamental importance. The total porosity represents the proportion of all pores, both closed and open, in the material and is calculated from the ratio between bulk density and mass density. Open porosity represents the portion of open, i.e., interconnected and mutually communicating pores in the total volume of the material. It can be deduced from the mass gain due to water imbibition into the porous material and can therefore be calculated as the product of the values of the water absorption capacity and the bulk density. A wide range of analytical methods have been used for studying the pore microstructure of porous media in recent years. These pore research techniques include both quantitative analysis and qualitative description of the pore space. The most commonly used methods for measuring pore characteristics include, in particular, optical microscopy, scanning electron microscopy, high-pressure mercury intrusion porosimetry, gas adsorption, X-ray computed micro-tomography (XCT), small-angle neutron scattering and nuclear magnetic resonance [3, 18–24]. A very simple method of describing the character of the rock pore space and the process of rock-water interaction, also indicating stone durability, is a long-term, time-dependent water saturation and evaporation [13, 15].

Permeability, which is closely connected with porosity, can be defined as the ability of porous material to allow the passage of a fluid. However, unlike porosity, this is a vector quantity and depends not only on the filtration properties of the porous medium (its structure, particle size, density, porosity, etc.), but also on the physical properties of the liquid, especially viscosity. Permeability is needed to predict flow and solute transport within porous material [17, 25]. Various methods can be used to determine the permeability of rocks, which differ in the medium used. In the case when the fluid passing through the porous material is water, permeability can be expressed by the coefficient of hydraulic conductivity k (m s^{-1}), which means a discharge velocity of water flow in a rock under the action of a unit hydraulic gradient [26]. If gas is used for measurement, the permeability of rocks is usually expressed in the form of a gas permeability coefficient K, which has the surface dimension (m^2) [25, 27].

Within the above methods of studying and characterizing the microstructure, XCT has become a very popular tool. In general terms, XCT represents a non-destructive 3D imaging and analysis technique for the investigation of internal structure of a wide range of objects and materials [28, 29]. XCT is currently widely used in the earth sciences for imaging rocks and determining their microstructure, such as anisotropy features, grain and pore size, rock cement distribution, crack parameters and development, hydraulic properties and fluid transport, often as part of a wider spectrum of analytical methods [29–36].

Sandstones have been widely used as a natural building material around the world for several millennia. For the purposes of the study, the Kocbeře sandstone was selected, which represents a traditional building stone of the Czech Republic. The aim of the study was to characterize the porosity and permeability of the Kocbeře sandstone, with regard to their spatial anisotropy and in relation to other microstructural and mineralogical parameters of the rock.

2 Material and methods
2.1 Rock material used in experiment
The building stone, used for the experiment, is represented by quartz-rich Cretaceous sandstone currently exploited in the Kocbeře quarry, approximately 25 km north from the city of Hradec Králové in northeastern Bohemia (50.4472397N, 15.8602975E). The Kocbeře sandstone has been utilized on Czech territory for construction, sculpture and decorative purposes for many centuries [37, 38]. More recently, it was used, for example, during the last repair of the Charles Bridge in Prague (2007–2010) in the form of replaced stone masonry blocks in the bridge's parapet wall [39]. Sandstone blocks for the preparation of test specimens were provided by the KOKAM Ltd. Company, the owner of the Kocbeře quarry.

2.2 Methods and equipment for sandstone characterization
Mineral and chemical composition and internal texture of the Kocbeře sandstone were studied using a relatively wide range of analytical methods, including optical polarization microscopy (OPM), scanning electron microscopy combined with energy dispersive spectroscopy (SEM/EDS), X-ray powder diffraction (XRPD), X-ray fluorescence (XRF) spectroscopy, mercury intrusion porosimetry (MIP), and hydraulic conductivity and gas permeability measurements.

OPM for basic petrographic analysis were undertaken in transmitted light on cover-slipped thin sections using a NIKON Eclipse LVDIA-N polarizing microscope (Nikon, Japan). Determination of quantitative representation of basic rock-forming minerals was carried out using a NIS Elements (Laboratory Imaging, Czechia) image analysis software [40].

As a supplement to OPM, SEM observations combined with EDS microanalyses were performed using a Vega 3 microscope (TESCAN, Czechia) equipped with

a tungsten cathode and an EDAX detector. The measurements were performed at a beam voltage of 30 keV, a current of 1–3 nA, and a high vacuum greater than 10^{-3} Pa. SEM/EDS microanalyses were applied for detail characterization of mineralogical composition and for observations of intensity of secondary silicification. SEM images were taken under backscatter (BSE) and secondary electrons (SE) conditions. Samples before imaging were gold sputtered in order to ensure adequate electron conductivity.

Analysis of mineralogical composition of sandstone matrix was carried out using XRPD by a Rigaku SmartLab diffractometer (Rigaku Corporation, Japan) with a D/teX Ultra 250 detector under the following conditions: cobalt tube (CoKα, $\lambda_1 = 0.178892$ nm, $\lambda_2 = 0.179278$ nm), voltage of 40 kV, current of 40 mA, 2Θ interval from 2° to 90°, step size of 0.01° 2Θ and measurement speed of 0.5° min^{-1}. The powder samples were gently grinded using agate mortar before analysis and pressed using microscope glass in a rotational sample holder and measured in the reflection mode (Bragg-Brentano geometry). The measured data were evaluated using PDXL 2 software (2.4.2.0) (Rigaku Corporation) [41] and compared with database PDF-2 [42] (International Centre for Diffraction Data, Newton Square, USA).

Chemical composition of the Kocbeře sandstones was determined semi-quantitatively using a XEPOS XRF energy dispersive spectrometer (Spectro, Germany). Analytic samples were prepared in the form of pressed pellets from a mixture of rock powder and wax. After trituration, the samples were placed in a plastic cuvette with a Mylar protective foil and then analyzed in a protective atmosphere (He). XRF, as well as SEM/EDS and XRPD analyses were performed by dr. Alexandr Martaus at VSB-Technical University of Ostrava.

An AUTOPORE 9500 mercury porosimeter (Micromeritics Instrument Corporation, USA) was used for the determination of open porosity and pore size distribution in sandstone. Testing samples with a volume of approximately 2000 mm^3 ($10 \times 10 \times 20$ mm) were applied for the analysis. MIP measurements were made by Soňa Študentová at VSB-Technical University of Ostrava.

Open (effective) porosity of the Kocbeře sandstone was also determined by calculation from the measured values of bulk density and water absorption capacity until the weight stabilizes according to the previously valid Czech technical standard ČSN 72 1155 [43]. Bulk density was calculated from the mass of the specimen and the bulk volume (the bulk volume of the specimen prepared in the form of regularly shaped cylinders was calculated by means of vernier calliper measurements). Water absorption capacity was calculated from the values of weights of dry and water saturated test specimens. The soaking time until the weight stabilized was approximately 4 weeks. The measurement was performed on cylindrical test specimens with a diameter of 48 mm and length of ca 96 mm, i.e., with length-to-diameter (L/D) ratio of 2:1. Test specimens were prepared in two directions with respect to the rock fabric anisotropy, both perpendicular (designated as "K" direction) and parallel (designated by the letter "P") to the bedding surface.

The measurements of hydraulic conductivity were carried out in a permeameter by the Infratest Prüftechnik GmbH (Germany) in the triaxial pressure chamber by deaerated pressurized water under the constant hydraulic gradient. Cylindrical test specimens with a diameter and length of 48 mm, i.e., L/D ratio of 1:1, were prepared for this measurement. The confining pressure was set at 0.55 MPa during the measurements. A hydraulic gradient of ca 80 was created in the sample (sample height is ca 48 mm; the difference in pressure column of water was set at 4 m). The calculated hydraulic conductivity coefficient (HCC) at the measurement temperature was subsequently recalculated to the comparative value for HCC k_{10} at 10 °C.

Gas permeability of the Kocbeře sandstone was measured using a KTK 100 triaxial cell (UNIPRESS, Poland) modified for gas passage [44]. The source of axial stress was the computer-controlled mechanical press ZWICK 1494 (Zwick/Roell, Germany) with the maximum force of 600 kN. Nitrogen was used as a measuring gas medium. Testing samples with 48 mm in diameter and ca 96 mm in length, i.e., with L/D ratio of 2:1, were covered with a rubber membrane, then clamped in jaws of the press machine and the confining pressure was set to the value of 3 MPa. Throughout the duration of the experiment, the nitrogen pressure was regulated using the control valve so that it was kept at the required value of 0.1 MPa.

2.3 Instrumentation and methodology of the XCT experiment

A non-destructive method of 3D XCT using a conical X-ray beam and a flat panel X-ray detector was used to study and analyze the pore space and permeability of Kocbeře sandstone. Radiographic images (input data for XCT volume reconstruction) were captured while rotating the sandstone sample through 360°. The obtained tomographic volume was further analyzed using digital image

processing methods and numerical methods utilizing the segmented tomographic volume to determine (calculate) the porosity and permeability of the studied sandstone.

An XTH 225 ST X-ray scanner (Nikon Metrology NV, Japan) was used for XCT scanning. Two cylindrical sandstone specimens (hereinafter referred to in the text as "sample No. 1" and "sample No. 2") with a diameter of 10 mm were scanned with a voxel size of 7.5 μm. A rotational method for 3D XCT scanning of sandstone was applied with the following scanner settings:

1. X-ray source 200 kV at 10 W;
2. 3142 radiographic projections with averaging of two radiographic image;
3. Exposure time of 1 radiographic image 1415 ms.

A virtual cubic volume was prepared from each scanned cylindrical XCT volume. A cubic XCT volume with a side size of ca 8.5 mm (ca 0.6 cm^3) was subsequently analyzed in the VGStudio Max 3.2 (VGS) software [45] (Volume Graphics GmbH, Germany) to determine open and effective porosity, permeability tensor as well as HCC.

The spatial resolution of the XCT data, defined by a voxel size of 7.5 μm, sets a fundamental lower limit on the size of pores and pore throats that can be reliably resolved. Pore features approaching the voxel size (approximately two to three voxels) are affected by partial volume averaging, meaning that individual voxels contain a mixture of pore space and solid matrix, resulting in intermediate grey values and increased segmentation uncertainty. Consequently, reliable segmentation in the present dataset is achieved for pore sizes of approximately 15–20 μm and larger. This resolution limit defines the lower threshold applied in the subsequent VGS-based analysis. Under these conditions, coarse pores (diameter > 15 μm) and the upper part of the macropore range (diameter 0.050–15.000 μm) are robustly resolved, collectively representing approximately 80% of the effective pore volume.

The porosity analysis was carried out in the "VGDefX/ Only Threshold" module in the VGS software [45]. The threshold value was analyzed and determined for both original and filtered CT data (using adaptive Gauss filter). Several segmentation strategies were tested. The final working threshold was selected not solely to maximize agreement with laboratory porosity measurements, but to ensure a realistic representation of pore connectivity and pore-throat geometry, constrained by SEM observations and pore-size distributions obtained from MIP. This approach prioritizes methodological transparency and reproducibility by reporting the range of plausible threshold values rather than relying on a single automated criterion.

Three approaches were applied to determine the threshold value:

1. Determination of the threshold value in the menu item "Surface determination" based on the observation of the visualization of the pore/grain boundary and operator experience (interval of the grey isovalue ca 100–130);
2. Determination of the threshold value by a conservative isovalue of 50% (mean material grey value + mean air grey value) in the "Surface determination" menu item – manual mode (grey isovalue ca 127);
3. Otsu method for determining the threshold value in two settings, i.e., for segmentation of the pores and sandstone matrix (binary image, grey isovalue 126 ± 3) and for the Otsu three-class segmentation for pores, sandstone cement and the sandstone grains (grey isovalue for pores segmentation 105 ± 2), see Figs. 1 and 2.
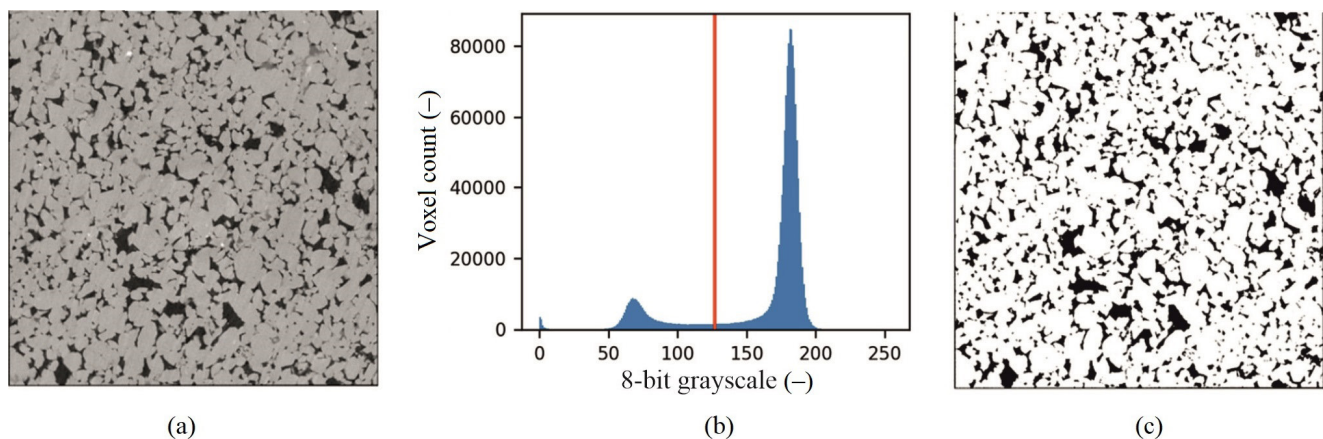

Fig. 1 Result of Otsu segmentation, two class segmentation for pores and sand–sized clasts: (a) original; (b) histogram; (c) Otsu result
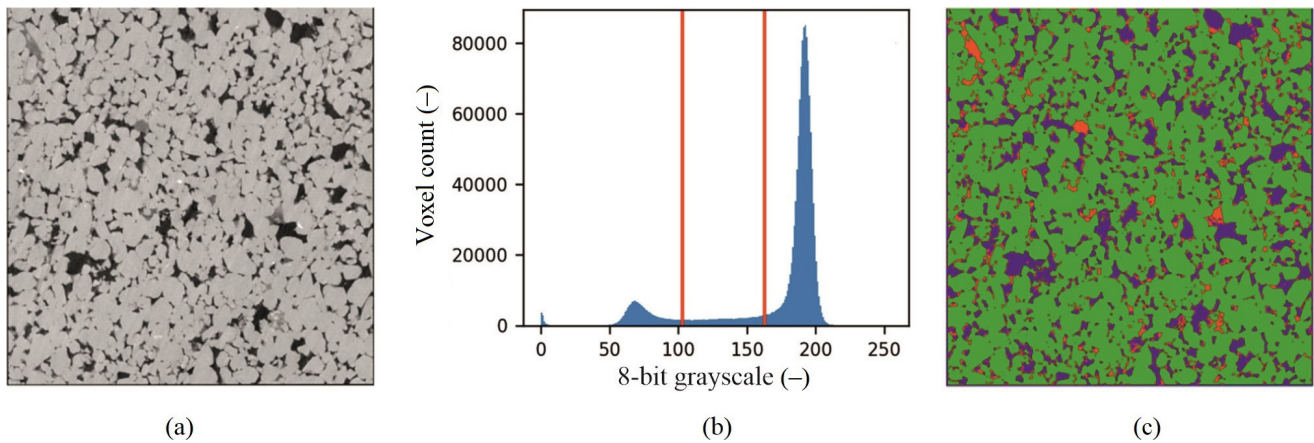
| (a) | (b) | (c) |

Fig. 2 Result of three phase Otsu segmentation for pores (blue), sandstone matrix and/or cement (red) and the sandstone grains (green): (a) original; (b) histogram; (c) Otsu result

The resulting sandstone porosity and its directional variability in analyzed samples determined from the range of threshold values found is shown in Figs. 3 and 4.
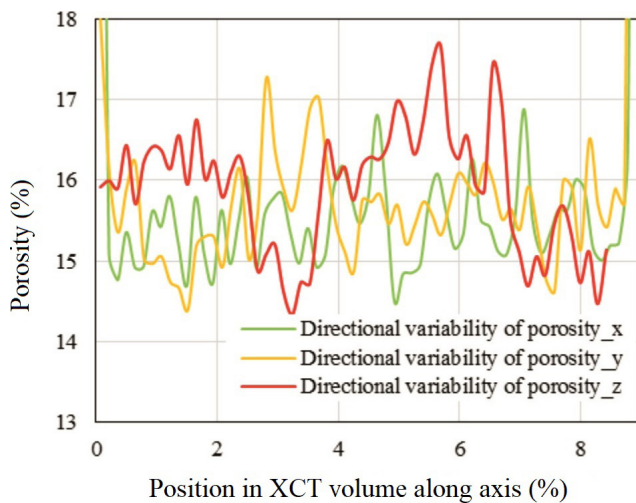

Fig. 3 Directional variability of sandstone porosity in sample No. 1 in the *x*, *y* and *z*-axis directions in the internal coordinate system of the XCT volume
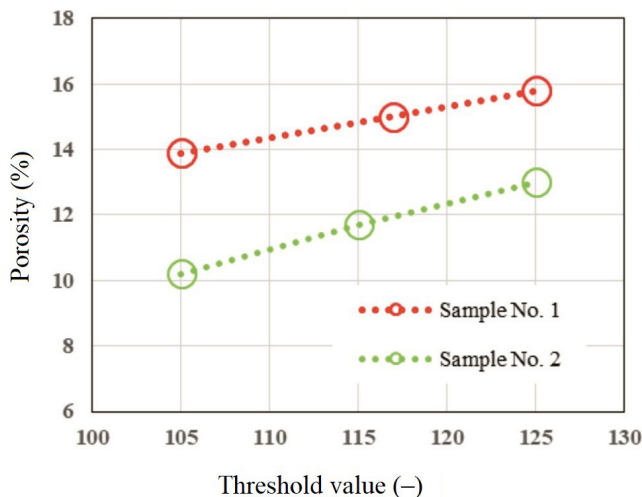

Fig. 4 Resulting sandstone porosity determined based on the found range of voxel threshold values in analyzed XCT volumes

The permeability analysis was performed using the "Transport Phenomena Simulation" module of the VGS software [45] to simulate fluid transport processes in porous materials based on Stationary low-Reynolds flow of an incompressible fluid through the voids of a porous material assumed to be completely filled with fluid. The analysis was carried out applying both the "Absolute Permeability Tensor (APT)" and the "Absolute Permeability Experiment (APE)" software items. The threshold value of 125 was used for the permeability analysis of the studied Kocbeře sandstone in APT analysis. The threshold value for pore space determination of 115 and 125 was used during the permeability analysis of the studied sandstone in APE analysis. Using APT, the 125 subvolumes were analyzed in each cubic XCT volume to assess inhomogeneity in the spatial distribution of porosity and permeability within the microstructure of the Kocbeře sandstone. APT analysis was performed for the entire XCT volume of the scanned sandstone too. For the purpose of representative elementary volume (REV) determination, APE analysis (liquid–water with a kinematic viscosity of 1 mPa s, pressure gradient ca 6000 Pa m^{-1}) was also realized for the XCT subvolumes.

3 Results and discussion
3.1 Composition, microstructure and properties of the Kocbeře sandstone
Based on OPM, SEM/EDS, XRPD and XRF analyses, Kocbeře sandstone can be characterized as fine- to medium-grained (according to the Wentworth classification [46]), moderately to poorly sorted psammitic rock with bimodal grain size distribution. It is composed of dominant (80 to 85% vol.) subangular to subrounded monocrystalline quartz grains with an average grain size (M_d) of 0.24 mm and maximum grain size (M_{max}) of up to 1.5 mm (Fig. 5). The rock framework components stable against weathering

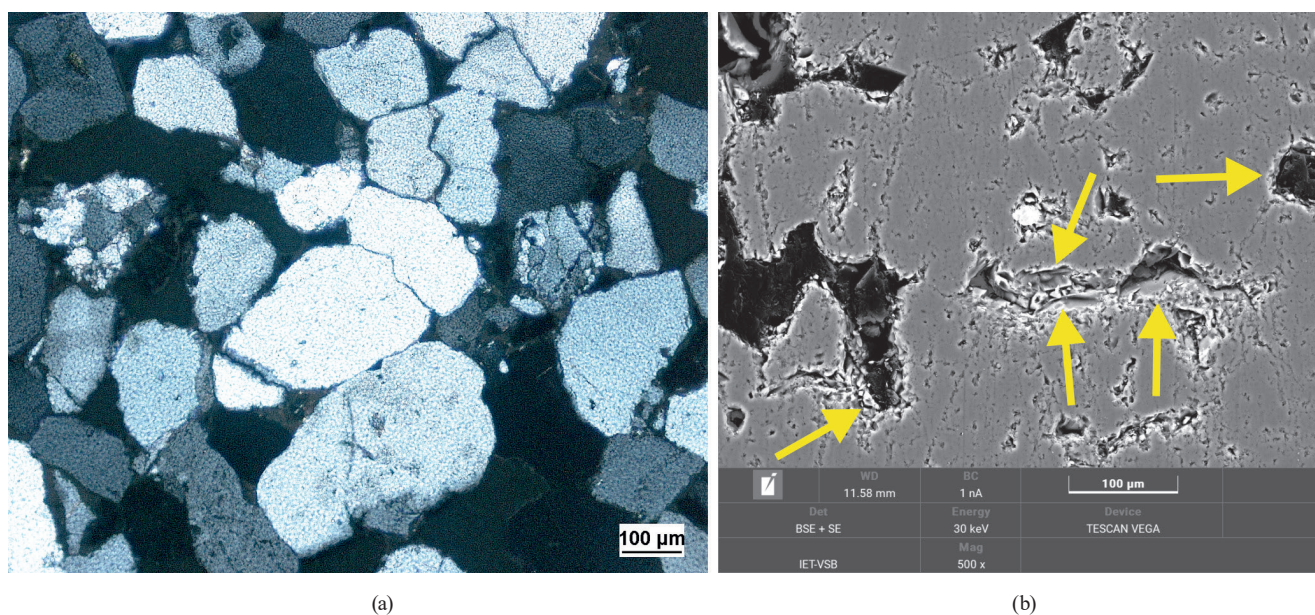(a)   (b)

Fig. 5 Micrographs of studied rock: (a) Grain-supported microtexture of the Kocbeře sandstone formed by quartz clasts with abundant concavo-convex to sutured contacts. OPM in transmitted light, crossed polarizers; (b) The overgrowths of secondary quartz (yellow arrows) around the grains rims. SEM, SE + BSE detectors

also include polycrystalline quartzite clasts with very variable microtexture. Their size and shape are similar to monocrystalline quartz (M_d = 0.28 mm), but they occur in a considerably smaller quantity. Non-stable clasts are represented by subangular to semioval feldspar grains (only orthoclase, ca 2% of rock volume, M_d = 0.26 mm, Fig. 6) and by scarce muscovite fragments (M_d = 0.27 mm). Zircon, tourmaline, rutile and apatite occur as accessory minerals. Interstitial constituents, i.e., matrix and rock cement (10–15% vol.) is formed by quartz which predominate over kaolinite (Fig. 7). In places, clay matter is penetrated by secondary Fe-oxyhydroxides. Very rare semioval

to oval light green glauconite grains with M_d of 0.11 mm can also be identified within the rock interstitial constituents. Secondary silicification within the rock is locally intense, the growth of authigenic quartz around grain rims is very common and in some cases can give the detrital quartz grain an angular up to euhedral crystal shape. This younger quartz also often grows into the original pore spaces between the grains and can even completely fill them. Silicification of clay matrix, authigenic quartz overgrowths onto detrital grains together with concavo-convex to sutured grain contacts (Fig. 5) indicate a relatively high degree of diagenesis of the Kocbeře sandstone.

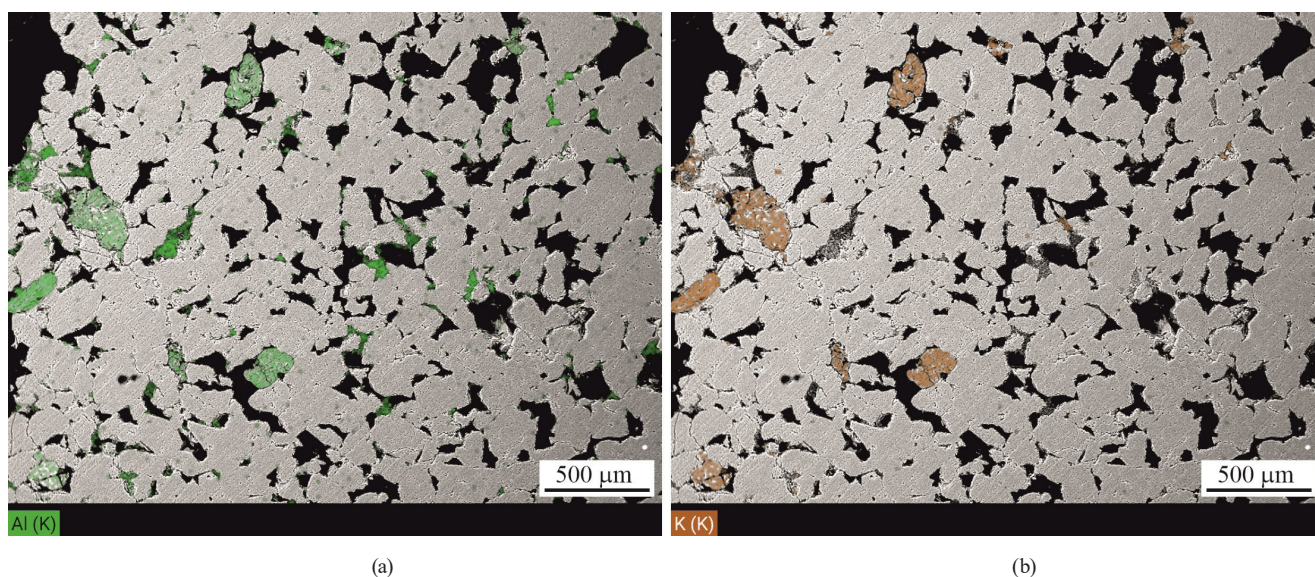(a)   (b)

Fig. 6 EDS mapping shows potassium feldspar grains in the BSE images. Potassium feldspar (orthoclase) contains both K^+ and Al^{3+} ions and is therefore identifiable at identical locations in both the Al map and the K map: (a) Al map; (b) K map
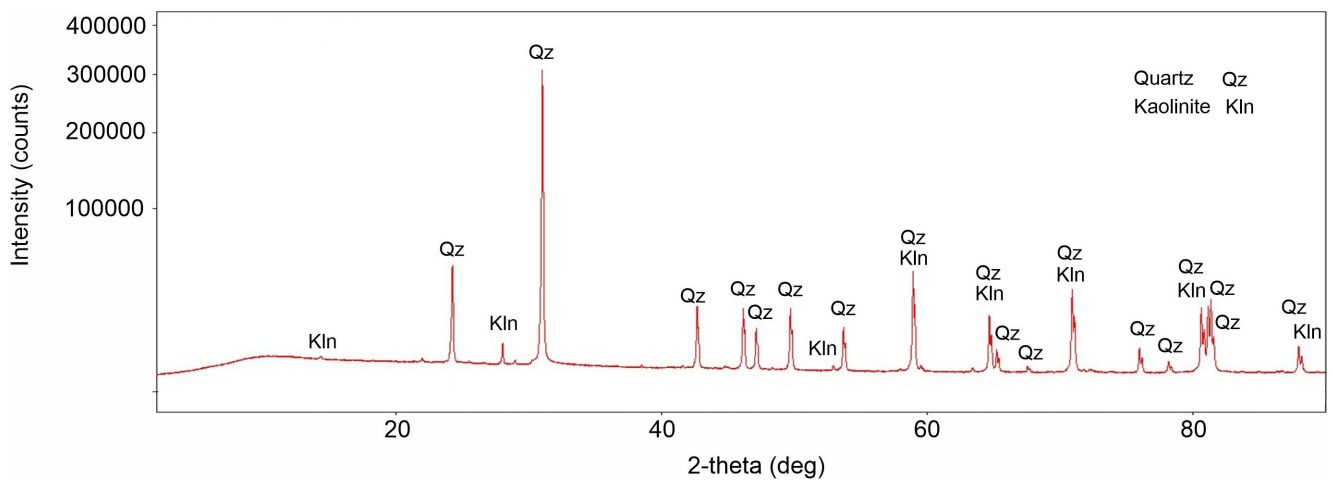
Fig. 7 XRPD patterns of the whole Kocbeře sandstone sample. Quartz as the main clastic component and kaolinite occurring in the sandstone matrix were identified

Identified mineralogical composition of the Kocbeře sandstone then corresponds to its chemical composition (Table 1). The very high SiO_2 content corresponds to the presence of quartz and other rock-forming silicates, aluminum and potassium are present in feldspars and muscovite. Iron oxides occur in Fe-oxyhydroxides, but also in some other minerals such as feldspars or glauconite.

The porosity and permeability of the Kocbeře sandstone were studied using MIP as well as laboratory measured open porosity, hydraulic conductivity and gas permeability (Tables 2 to 5).

As can be seen from the Table 2, studied Kocbeře sandstone is a macroporous material [47] with a wide range of pore sizes, with coarse pores over 15 μm being the most represented. The values of its open porosity measured *via* MIP vary in the interval of ca 12 to 17%. Completely similar open porosity values in the range of approximately 14 to 17% were also found by calculation from the values of bulk density and water absorption capacity (Table 3). Compared to other Czech Cretaceous sandstones used in construction [38, 48], the Kocbeře sandstone can thus be characterized by a relatively low to medium level of porosity. Concerning the laboratory determined values of HCC (orderly 10^{-6} to 10^{-8} m s^{-1}, see Table 4), the Kocbeře sandstone can be characterized as the rock with moderate to low hydraulic conductivity in terms of classification by Singhal and Gupta [49]. The determined values of porosity and HCC are in a good agreement with the data published for the Kocbeře sandstone in Šperl and

Trčková [26]. Regarding the detected values of gas permeability coefficient, which are mostly in the order of 10^{-12} m^2 (Table 5), the Kocbeře sandstone can be classified as moderately permeable rock according to above classification of Singhal and Gupta [49].

The described mineralogical composition and microtexture of the Kocbeře sandstone are then reflected in its material parameters (Table 6) [38, 48, 50–52].

In terms of the physical and mechanical properties given in Table 6, the Kocbeře sandstone can be characterized as sandstone having a moderate value of bulk density, a low to moderate absorption capacity and total porosity, relatively high abrasion resistance in laboratory conditions and moderate to high values of strength properties and fracture toughness. At the same time, the data presented in Tables 2, 3 and 6 show that the values of total porosity and open porosity are practically identical. This makes it clear that the vast majority of pores in the Kocbeře sandstone are formed by open, i.e., mutually communicating pores accessible to the influence of fluids and dissolved salts.

3.2 Experimental results of XCT analysis

The results of the XCT data analysis for both sandstone samples (sample No. 1 and sample No. 2) showed that, although they are the same rock type (fine- to medium-grained Kocbeře sandstone with a predominance of quartz clasts and secondary silicification), the findings point to pronounced microscopic heterogeneity of the pore structure and, consequently, of the transport properties (see Fig. 8,

Table 1 Chemical composition of the Kocbeře sandstone determined using XRF spectrometry (%)

SiO$_2$	TiO$_2$	Al$_2$O$_3$	Fe$_2$O$_3$*	MnO	MgO	CaO	Na$_2$O	K$_2$O	P$_2$O$_5$	LOI	Σ
95.78	0.08	2.17	1.19	0.01	0.01	0.00	0.01	0.24	0.02	0.31	99.82

Notes: * = iron in the form of Fe$_2$O$_3$; LOI = loss-on-ignition; the samples were burned in a muffle furnace for 3 h at 1100 °C

Table 2 Pore space parameters of the Kocbeře sandstone measured using MIP

Sample	V_{mmc} (mm^3 g^{-1}) % of total vol.	V_{me} (mm^3 g^{-1}) % of total vol.	V_{ma} (mm^3 g^{-1}) % of total vol.	V_{cp} (mm^3 g^{-1}) % of total vol.	r (µm)	P_{MIP} (vol. %)
Kocbeře 1	59.465	3.747	8.181	47.537	0.17	12.5
	100	6.30	13.76	79.94		
Kocbeře 2	81.698	3.163	27.857	50.678	0.28	17.2
	100	3.87	34.10	62.03		
Kocbeře 3	61.356	1.886	8.409	51.061	0.31	13.0
	100	3.07	13.71	83.22		
Kocbeře 4	57.126	1.776	7.813	47.537	0.27	12.1
	100	3.11	13.68	83.21		
Kocbeře 5	81.879	2.975	28.028	50.876	0.34	16.6
	100	3.63	34.23	62.14		
Kocbeře 6	58.227	1.820	17.310	39.097	0.40	12.0
	100	3.13	29.73	67.14		
Kocbeře 7	70.824	0.737	17.876	52.211	0.64	15.4
	100	1.04	25.24	73.72		
Arithmetic mean		3.45	23.49	73.06	0.34	14.1
Standard deviation		1.44	8.92	8.70	0.14	2.0
Coefficient of variability		41.7	38.0	11.9	41.2	14.2

Notes: V_{mmc} = volume of all pores measured by MIP (total intrusion volume), V_{me} = volume of mesopores (diameter 0.002–0.050 µm), V_{ma} = volume of macropores (diameter 0.050–15.000 µm), V_{cp} = volume of coarse pores (diameter over 15.000 µm), r = average pore diameter (4V/A), P_{MIP} = porosity determined by MIP (pore's nomenclature and boundaries between the individual pore size categories were adopted from the IUPAC terminology [47])

Table 3 Open porosity of the Kocbeře sandstone calculated from bulk density and water absorption capacity

Direction towards bedding planes	Sample	Weight of dry specimen (g)	Weight of saturated specimen (g)	Bulk density (kg m^{-3})	Water absorption capacity (%)	Open porosity (%)
Perpendicular	Kocbeře/K1D	205.20	219.85	2199	7.1	15.7
	Kocbeře/K2D	216.14	229.15	2270	6.0	13.6
	Kocbeře/K3D	207.12	223.00	2186	7.7	16.8
Parallel	Kocbeře/P1D	209.57	224.74	2202	7.2	16.0
	Kocbeře/P2D	211.93	226.33	2212	6.8	15.1
	Kocbeře/P3D	205.58	220.60	2206	7.3	16.2

Table 4 Coefficient of hydraulic conductivity of the Kocbeře sandstone at 10 °C (k_{10})

Direction towards bedding planes	Sample	Number of measurements	k_{10} (m s^{-1}) – average value	k_{10} (m s^{-1}) – minimum value	k_{10} (m s^{-1}) – maximum value
Perpendicular	Kocbeře/K1	6	2.54×10^{-6}	2.28×10^{-6}	2.85×10^{-6}
	Kocbeře/K2	6	3.95×10^{-8}	3.46×10^{-8}	4.47×10^{-8}
	Kocbeře/K3	6	1.43×10^{-6}	1.25×10^{-6}	1.50×10^{-6}
Parallel	Kocbeře/P1	2	4.13×10^{-6}	4.10×10^{-6}	4.15×10^{-6}
	Kocbeře/P2	2	6.31×10^{-7}	6.06×10^{-7}	6.56×10^{-7}
	Kocbeře/P3	2	6.08×10^{-6}	5.80×10^{-6}	6.36×10^{-6}

Table 5 Coefficient of gas permeability of the Kocbeře sandstone (K)

Direction towards bedding planes	Sample	K (m^2)	Direction towards bedding planes	Sample	K (m^2)
Perpendicular	Kocbeře/K4D	4.89×10^{-13}	Parallel	Kocbeře/P4D	3.22×10^{-12}
	Kocbeře/K5D	5.12×10^{-12}		Kocbeře/P5D	6.76×10^{-12}
	Kocbeře/K6D	1.04×10^{-12}		Kocbeře/P6D	1.89×10^{-12}

Table 6 Basic physical and mechanical properties of the Kocbeře sandstone according to various authors [38, 48, 50–52]

Parameter	Value (minimum–maximum)
Mass density (kg m^{-3})	2630–2670
Bulk density (kg m^{-3})	2140–2270
Total porosity (%)	12.0–17.2
Water absorption capacity by weight (%)	2.2–6.1
Ultrasonic P-wave velocity (dry sample) (km s^{-1})	2.74–3.48
Uniaxial compressive strength (dry sample) (MPa)	56–87
Dynamic Young's modulus (GPa)	17.2–24.7
Poisson's ratio (–)	0.16–0.33
Flexural strength (dry sample) (MPa)	5.9–7.9
Splitting tensile strength (dry sample) (MPa)	2.6–6.1
Fracture toughness–chevron bend test (dry sample) (MPa m$^{1/2}$)	0.73–0.98
Abrasion resistance by the Böhm method (mm)	2.6–3.1
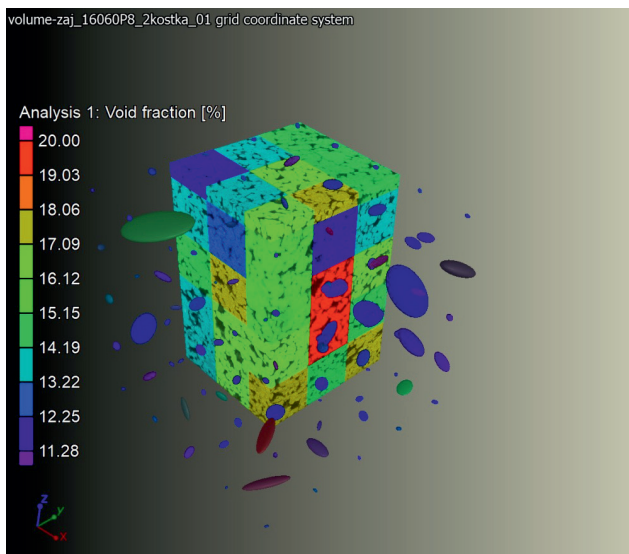
Fig. 8 Spatial distribution of porosity and permeability tensors in sample No. 1

which depicts the permeability-vector ellipsoids and the variability of porosity in the individual subvolumes).

The porosity values determined from the XCT analysis range from approximately 10 to 16% in both cases, depending on the chosen threshold value used to delineate pores in the tomographic data (see, for example, Fig. 4 and Table 7). The XCT-derived porosity results exhibit a natural directional variability of porosity within the rock (see Fig. 3), fluctuating within the range of 4%. Variability of porosity is also evident from the laboratory tests (see Tables 2 and 3). The porosity values obtained from the

XCT analysis correspond to the range of the laboratory measurements, i.e., about 13.6–16.8% (see Table 3) and 12.0–17.2% (see Table 2), respectively.

It can be concluded that permeability exhibits a higher degree of variability (60–90%) than porosity (see Table 7). For sample No. 1, the average value of absolute permeability in the analyzed subvolumes was 5.84×10^{-12} m^2, while in the analysis of the entire volume it decreased to 2.91×10^{-12} m^2. For sample No. 2, the values were similar (6.21×10^{-12} m^2 vs. 3.29×10^{-12} m^2). This fact points to the phenomenon of scale effect – when evaluating smaller volumes (125 subvolumes), the presence or absence of local permeable channels with higher permeability is likely to have an impact, while in the entire volume, the heterogeneity of the occurrence of these channels is averaged out and the resulting permeability may be lower.

The results of permeability analysis on XCT data demonstrated the anisotropy of permeability transport properties of the analyzed building sandstone, such as permeability and hydraulic conductivity. Numerical simulations showed that the values of the main tensor components of permeability K_{xx}, K_{yy}, and K_{zz} (see Table 7), respectively HCC (see Table 7), differ from each other by approximately 15–40% (see Fig. 8 and Table 8). The anisotropy of HCC was also confirmed, although to a different extent, based on the results of laboratory measurements of HCC in the perpendicular and parallel directions to the layering of Kocbeře sandstone. The average HCC value in the parallel direction is approximately 170% higher than in the perpendicular direction (see Table 3). Goupil et al. [53] also states that the normal range for sandstones in the parallel direction to lamination is approximately 30–130% higher than in the perpendicular direction (ratio $k∥/k⊥ ≈ 1.3–2.3$). The variability of permeability between directions may indicate the importance of microscopic textural differences, such as the influence of irregular cementation and secondary silicification, which can selectively seal pores and thus change the directions of preferential flow. The coefficients of variability (CV) in APT analysis reach high values (approximately 60–90%, see Table 7), confirming significant internal heterogeneity. This is probably consistent with observations from microstructural analysis, where it was found that the intensity of secondary silicification is not uniform in space and can lead to local contrasts (differences) in permeability values.

Based on APT analysis in individual subvolumes, it was found that porosity values are not a reliable variable indicator for predicting permeability of the analyzed sandstone. The correlation between porosity and hydraulic

Table 7 Average values of permeability and its basic statistical data from the performed APT analysis of 125 XCT subvolumes

Sample		Porosity (%)	Mean absolute permeability K (m²)	Mean hydraulic conductivity k (m s⁻¹)	Absolute permeability tensor K_{xx} (m²)	Hydraulic conductivity k_{xx} (m s⁻¹)	Absolute permeability tensor K_{yy} (m²)	Hydraulic conductivity k_{yy} (m s⁻¹)	Absolute permeability tensor K_{zz} (m²)	Hydraulic conductivity k_{zz} (m s⁻¹)
Sample No. 1	A.M.	15.2	5.84×10^{-12}	4.39×10^{-5}	5.59×10^{-12}	4.19×10^{-5}	6.89×10^{-12}	5.17×10^{-5}	5.06×10^{-12}	3.80×10^{-5}
	SD	1.6	3.57×10^{-12}	2.68×10^{-5}	3.80×10^{-12}	2.85×10^{-5}	4.77×10^{-12}	3.58×10^{-5}	3.09×10^{-12}	2.32×10^{-5}
	CV (%)	10.7	61.1	61.1	68.0	68.0	69.3	69.3	61.0	61.0
Sample No. 1 – whole XCT volume analysis		15.3	2.91×10^{-12}	2.18×10^{-5}	2.73×10^{-12}	2.05×10^{-5}	3.60×10^{-12}	2.71×10^{-5}	2.39×10^{-12}	1.8×10^{-5}
Sample No. 2	A.M.	13.2	6.21×10^{-12}	4.66×10^{-5}	6.97×10^{-12}	5.23×10^{-5}	6.28×10^{-12}	4.71×10^{-5}	5.37×10^{-12}	4.03×10^{-5}
	SD	1.6	4.89×10^{-12}	3.67×10^{-5}	6.06×10^{-12}	4.55×10^{-5}	5.75×10^{-12}	4.32×10^{-5}	3.99×10^{-12}	3.00×10^{-5}
	CV (%)	12.1	78.7	78.7	86.9	86.9	91.6	91.6	74.4	74.4
Sample No. 2 – whole XCT volume analysis		13.4	3.29×10^{-12}	2.47×10^{-5}	3.86×10^{-12}	2.90×10^{-5}	3.21×10^{-12}	2.41×10^{-5}	2.8×10^{-12}	2.1×10^{-5}

Note: A.M. = arithmetic mean, SD = standard deviation, CV = coefficient of variability

Table 8 Values of permeability ratios K_{xx}/K_{yy}, K_{xx}/K_{zz} and K_{yy}/K_{zz} in the analyzed directions of the internal coordinate system x, y and z, APT analysis results of the 125 XCT subvolumes

Sample		Porosity (%)	Ratio of absolute permeability tensor K_{xx}/K_{yy} (–)	Ratio of absolute permeability tensor K_{xx}/K_{zz} (–)	Ratio of absolute permeability tensor K_{yy}/K_{zz} (–)
Sample No. 1 – XCT subvolumes analysis	A.M.	15.2	1.31	1.16	1.43
	SD	1.6	0.45	0.54	0.61
	CV (%)	10.7	34.2	46.6	42.6
Sample No. 1 – Whole XCT volume analysis		15.3	1.32	1.14	1.51
Sample No. 2 – XCT subvolumes analysis	A.M.	13.2	1.25	1.35	1.20
	SD	1.6	0.60	0.62	0.55
	CV (%)	12.1	47.82	45.85	45.57
Sample No. 2 – Whole XCT volume analysis		13.4	1.20	1.38	1.15

Note: A.M. = arithmetic mean; SD = standard deviation; CV = coefficient of variability

conductivity coefficient is very low (see Fig. 9); the decisive factor will be the complex geometry of the pore system in the sandstone.

APE numerical simulations of fluid flow in a porous sandstone environment (pressure gradient approximately 6000 Pa m⁻¹; liquid–water with a kinematic viscosity of 1 mPa s) also showed that the output parameters are strongly influenced by the size of the analyzed volume. In small subvolumes, parameter fluctuations occur. In larger volumes, however, the values stabilize and tend toward representative values for the rock as a whole (see Figs. 10 and 11). This analysis showed that the differences in effective porosity in relation to total porosity are very small, approximately up to 1%. The ratio of these porosities is about 99%, which indicates that almost all
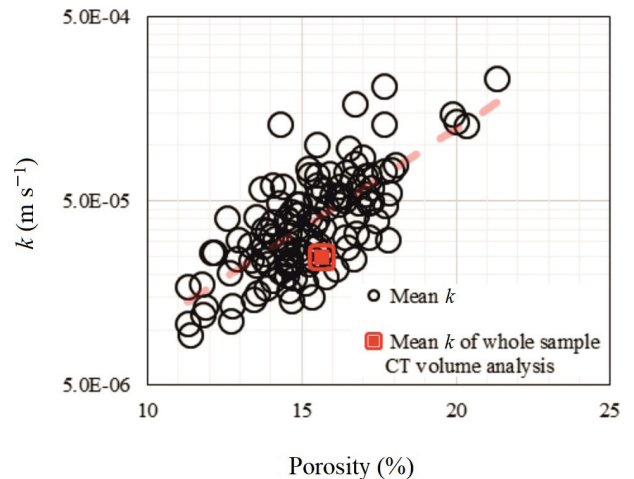

Fig. 9 Sample No. 2: the mean values of HCC (k) for each 125 XCT subvolumes plotted against their porosity values
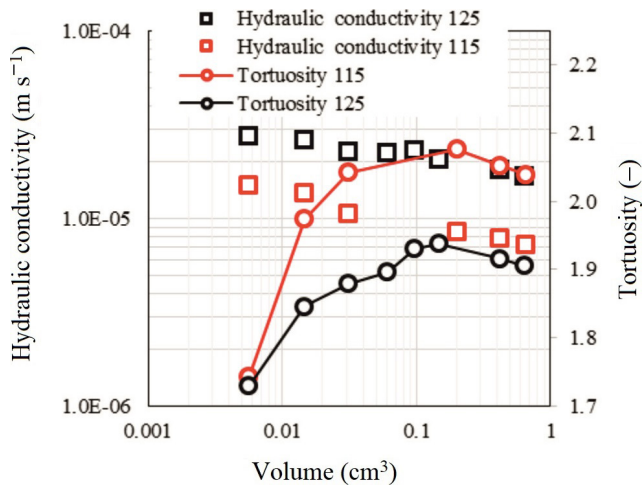
Fig. 10 Sample No. 1: HCC and tortuosity values from the results of APE analysis depending on the investigated XCT volume, analyzed at threshold values 115 and 125
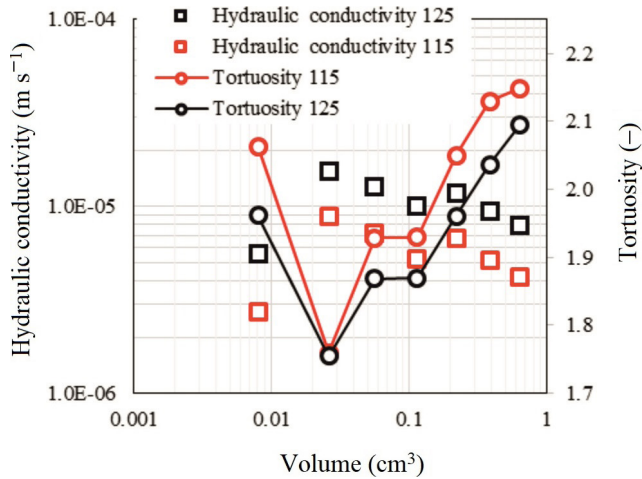

Fig. 11 Sample No. 2: HCC and tortuosity values from the results of APE analysis depending on the investigated XCT volume, analyzed at threshold values 115 and 125

Fig. 12 Sample No. 1: result of APE analysis, development of whole (total) and effective porosity in direction of liquid flowing (analyzed volume 0.42 cm³)

Fig. 13 Sample No. 2: result of APE analysis, development of whole (total) and effective porosity in direction of liquid flowing (analyzed volume 0.64 cm³)

pores are interconnected and form a hydraulically effective network (see Figs. 12 and 13). The same finding was obtained when determining total porosity and open (effective) porosity using common laboratory measurements (see Tables 2, 3 and 6). The tortuosity values range between 1.9 and 2.1. This means that the flow path is approximately 1.9 to 2.1 times longer than the shortest geometric distance between the interconnected pores on the sides of the sample through which the liquid enters and exits. With increasing analyzed volume, tortuosity increases slightly, reflecting the complexity of the pore network and confirming that the fluid flow is not completely linear (straight). The HCC shows higher variability in small subvolumes (on the order of 10^{-5} to 10^{-6} m s^{-1}) and the values even out with increasing volume. This phenomenon corresponds to the scale effect, where locally well-connected pores can increase conductivity, but in larger volumes these
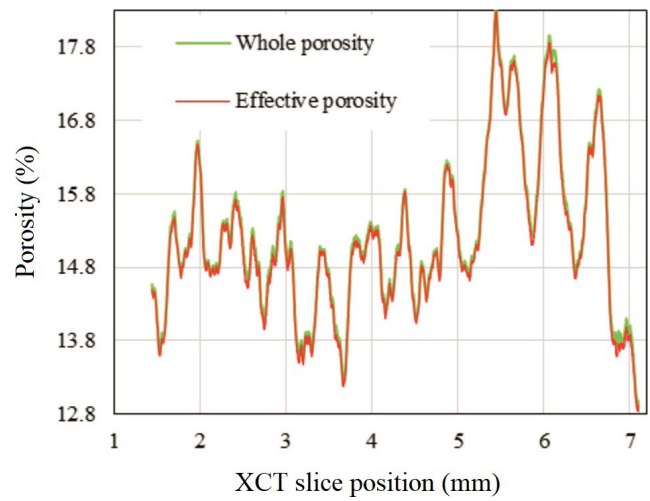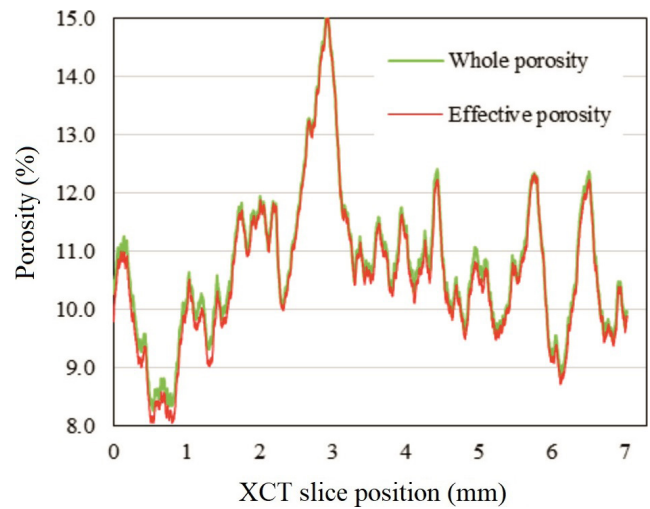
channels are averaged out with less permeable zones. The results show that at a volume of around 0.4–0.6 cm³, the values of permeability, porosity and tortuosity begin to stabilize and the variability between calculations decreases. This range can therefore be designated as the REV for a given type of sandstone with a given quality of XCT data in a first approximation. At smaller volumes, the dispersion is higher and the values may not reliably represent the properties of the rock. For sample No. 2, the level of stabilization of the analyzed values is less conclusive, probably due to its higher heterogeneity and lower porosity, and thus a more complicated pore space in which flow occurs (see Fig. 11).

Figs. 14 and 15 shows the fluid flow velocity in the analyzed sandstone sample based on the results of APE
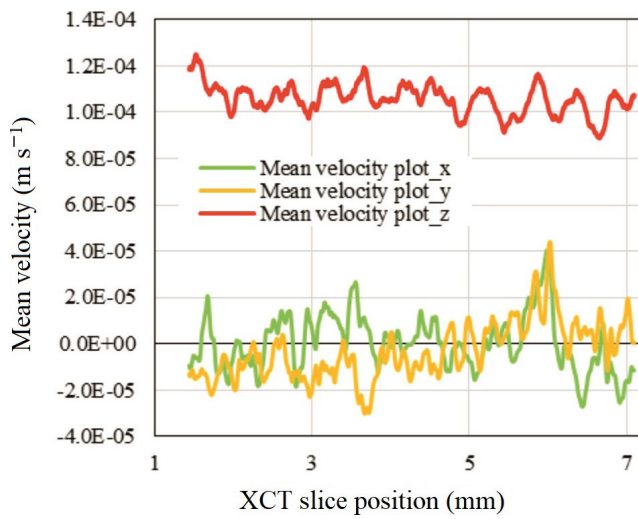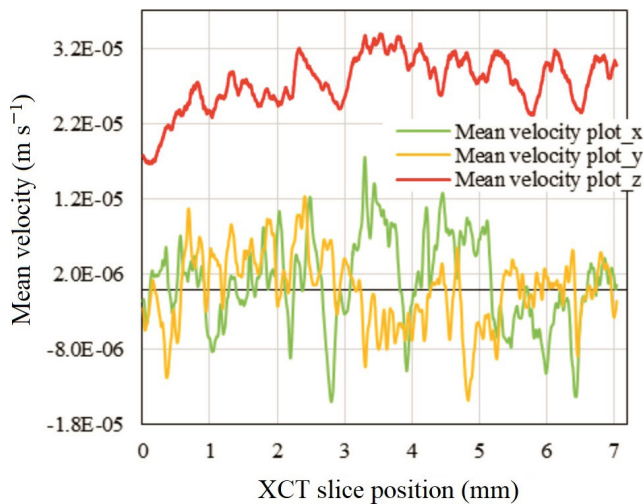
Fig. 14 Sample No. 1: fluid flow velocity in the analyzed sandstone sample based on the results of APE numerical simulation in the three analyzed directions x, y, and z (analyzed volume 0.42 cm^3)

Fig. 15 Sample No. 2: fluid flow velocity in the analyzed sandstone sample based on the results of APE numerical simulation in the three analyzed directions x, y, and z (analyzed volume 0.64 cm^3)

numerical simulation in the three analyzed directions x, y, and z. The z-direction represents the direction of the pressure gradient acting in the fluid, which is also reflected in the distribution of the mean fluid flow velocities. For sample No. 1, the average velocity in the z-direction is of the order of 1×10^{-4} m s^{-1}, while for sample No. 2, the average flow velocity in the z-direction is lower, approximately 2.5×10^{-5} m s^{-1} (see Figs. 14 and 15), which corresponds to the porosity values at both samples. This trend in fluid flow velocity is also maintained in the x- and y-directions. The tortuosity and relatively complex geometry of the pore space probably influence the positive and negative fluctuations in the average flow velocity in the transverse direction relative to the main flow direction (z-direction) at both analyzed samples. These directional fluctuations

are the result of the fluid flowing around the grains. This flow has an effect on the change in direction and nonlinear flow of the liquid in the intergranular channels, which are formed by the morphology and composition of the grains in the analyzed sandstone. The degree of oscillation of the directional flow velocity can be an informative characteristic of the complexity of the pore space of geomaterials in general. Fig. 16 represents the nature of fluid flow through the pore space of Kocbeře sandstone using streamlines, which reflect its geometric habitus. The streamlines represent a visual tool used in fluid dynamics (hydromechanics) to display the instantaneous direction of velocity of fluid particles (liquid or gas) at a given moment. A higher density of streamlines (their mutual distance) indicates a higher fluid flow velocity in sandstone, and conversely, where they are further apart (lower density), the velocity is lower. The fluid flow velocity is also highlighted in color in Fig. 16. The highest flow velocities are represented by red shades, for example in areas of sandstone corresponding to "intergranular pore throats" (see 2D XCT slice in Figs. 16 (a) and (b)). The streamlines reflect its geometric habitus of fluid flow through the pore space of sandstone whose tortuosity values range between 1.9 and 2.1.

The XCT-based porosity and permeability characteristics obtained for the Kocbeře sandstone are consistent with trends reported in previous international XCT studies of sandstones. Earlier investigations demonstrated that pore-network connectivity, topology, and microstructural heterogeneity exert a stronger control on transport properties than bulk porosity alone [33, 34]. Similar conclusions regarding permeability anisotropy and scale-dependent behavior have been reported for sandstones combining XCT with numerical transport simulations [35, 36]. These observations align well with broader applications and limitations of XCT in sandstone pore characterization [28] and with recent XCT-based analyses of building sandstones addressing pore-scale heterogeneity and transport-related properties [30].

4 Conclusions

Based on the pore space and permeability analysis of the Kocbeře sandstone carried out on the XCT data and compared with the results of MIP and other laboratory techniques, the following main conclusions can be drawn:

- A very good agreement was observed between the average values of open porosity determined by XCT imaging analysis (approximately 13% and 15%, respectively), MIP measurements (14 ± 2%) and calculation from bulk density and water absorption

(a)   (b)
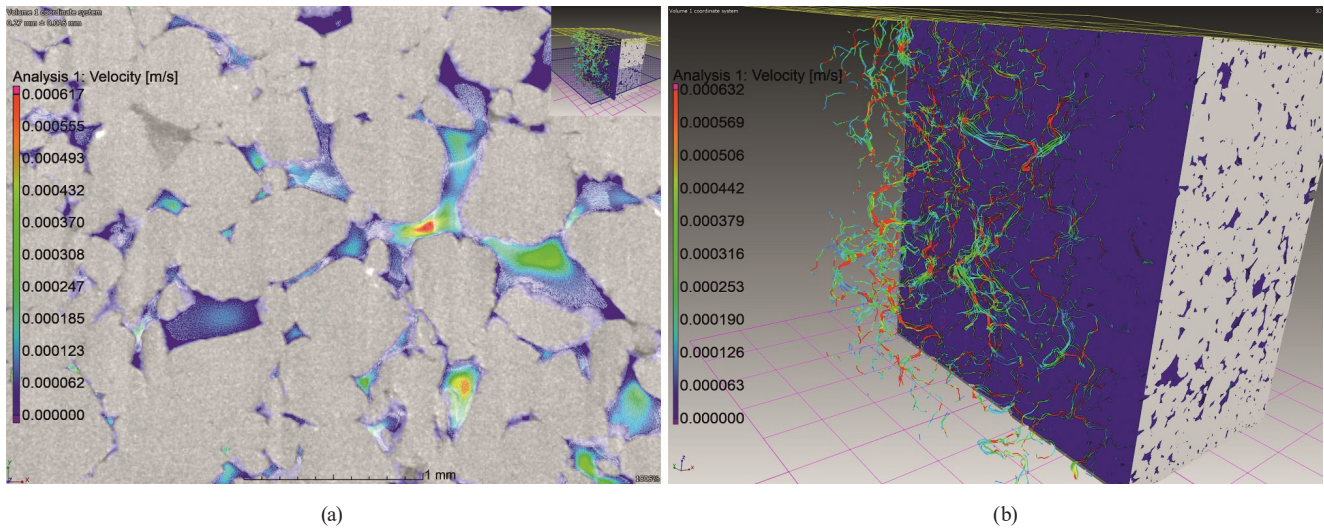
Fig. 16 Illustrative visualization of typical flow patterns and flow velocity in sample No. 2 using streamlines (APE analysis): (a) 2D XCT slice;
(b) 3D image of tomographic volume (the bottom plane with a purple square grid represents the entry of liquid into the analyzed volume, while the
upper plane with a yellow square grid represents the exit of liquid from the analyzed volume)

capacity (ca 14% to 17%). Minor differences between XCT- and MIP-derived pore characteristics arise from the different resolution ranges and physical principles of both methods, which capture complementary parts of the pore system rather than being directly interchangeable. Together, the combined interpretation of XCT and MIP results provides a robust basis for characterizing the effective pore space and its heterogeneity in the studied sandstone. However, XCT, thanks to the possibility of 3D data reconstruction, revealed considerable heterogeneity of porosity in the individual analyzed subvolumes (see Figs. 3 and 8).

• Regarding the permeability analysis, an order of magnitude agreement was found between the results of laboratory gas permeability measurements (10^{-12} to 10^{-13} m^2) and the calculation of water permeability from XCT scanning (10^{-12} m^2), even though fluids of different viscosities were used. On the contrary, the average HCC values from laboratory measurements (in the order of 10^{-6} to 10^{-8} m s^{-1}) are not in good agreement with the results of XCT data analysis (in the order of 10^{-5} m s^{-1}). This discrepancy will be the subject of further investigation.

• Similar to porosity, a very significant inhomogeneity was also observed in the spatial distribution of permeability tensors calculated for the individual subvolumes. The coefficient of variation of the permeability values determined in these 125 subvolumes reaches ca 60 to 90% (see Table 7). The considerable dispersion of porosity and permeability values of the Kocbeře sandstone at the microscale is given

by its microstructure. In particular, intense secondary silicification occurs here, which unevenly affects the clay sandstone matrix.

• The spatial anisotropy of the permeability of the Kocbeře sandstone in the analyzed x, y and z directions, expressed by the ratios K_{xx}/K_{yy}, K_{xx}/K_{zz} and K_{yy}/K_{zz}, ranges from approximately 1.16 to 1.43 (see Table 8).

• It can be concluded that the calculated HCC values do not correlate reliably with the open porosity of the Kocbeře sandstone (Fig. 9). The resulting hydraulic conductivity of the rock is probably significantly influenced by the complexity of fluid flow through their pore system (e.g., tortuosity, see Figs. 10 and 11) and other geometrical characteristics of the pore system.

• As stated above, HCC of Kocbeře sandstone determined by laboratory measurements ranges from ca 1×10^{-6} to 4×10^{-8} m s^{-1}. The HCC values calculated from XCT data using APE analysis are distributed in the interval of ca 2×10^{-5} to 6×10^{-6} m s^{-1} and are determined in the REV region (Figs. 10 and 11). The several-order-of-magnitude discrepancy between HCC derived from pore-scale XCT simulations and laboratory measurements is interpreted as a fundamental scale mismatch rather than a methodological error. The limited XCT sample volume does not fully capture the statistical representation of larger-scale flow-limiting and flow-enhancing features, such as connected larger pores, microcracks, or structural heterogeneities, which exert a dominant control on bulk permeability. Under laboratory conditions, rock cores with volumes on the order of 100 cm^3 are tested,

whereas XCT-based analyses are performed on volumes of approximately 0.7 cm^3 in order to resolve detailed pore geometry. Consequently, permeability derived from XCT should be interpreted primarily in a relative sense, suitable for assessing permeability anisotropy and microstructural controls on flow, whereas laboratory measurements remain essential for quantifying absolute HCC. Bridging this scale gap requires multi-scale workflows combining XCT, MIP, SEM observations, and laboratory future permeability testing across increasing sample volumes.

XCT numerical analysis confirmed a high degree of connectivity of the pore system – effective porosity reaches almost the same values as total porosity. The findings confirm that, in order to reliably evaluate the transport properties of sandstones, it is necessary to combine XCT numerical simulations with laboratory tests on larger volumes. The weak correlation between porosity and hydraulic conductivity indicates that volumetric porosity alone does not adequately describe fluid-flow behavior. Permeability is instead governed by pore-network microstructural characteristics such as pore connectivity, coordination number, tortuosity, critical pore-throat radius, and the quality and geometry of flow channels [54]. A quantitative assessment of these connectivity-related parameters and potential fractal characteristics of the pore network would provide additional insight, but lies beyond the scope of the present study. The values of hydraulic conductivity and tortuosity are strongly dependent on the scale (volume) of the XCT analysis – they are more scattered in small volumes, while in REV they settle at lower values closer to laboratory measurements. The results confirm that numerical simulation in the VGS environment provides valuable insight into the microstructure-dependent variability of sandstone permeability, but for practical applications, it is necessary to carefully select the size of the analyzed volume with regard to computational complexity and reliability of results. Numerical simulations show a strong increase in computation time with increasing analyzed volume, ranging from hundreds of seconds for small subvolumes to more than 24 h for the largest XCT volumes, depending on available computing resources. This behavior reflects the inherently high computational demands of high-resolution pore-scale flow simulations, in which memory usage and computation time scale nonlinearly with sample size and voxel resolution. Practical application therefore requires a compromise between analyzed volume, spatial resolution, and time feasibility, which can be alleviated by representative elementary volume (REV) analysis, region-of-interest selection, and the use of parallelized solvers on multicore or high-performance computing platforms.

To sum up, the XCT represents an effective and useful complementary technique to the existing commonly used methods in comprehensive study of porosity and permeability of porous building materials. Like any other laboratory method, XCT has its advantages, but also its limits. The limitation is the size of the scanned sample used, which significantly affects the resulting resolution. From this point of view, XCT only provides information about the presence of pores of a size that includes a portion of macropores and coarse pores. The distinct advantage is the possibility of 3D imaging and reconstruction of the microstructure. At the same time, contrary to, for example, mercury porosimetry, XCT is a non-destructive method, so the samples are reusable for any further laboratory study. In conclusion, XCT is a powerful technique in many research areas of geomaterials characterization, for example in the respect of their degradation due to the influence of the surrounding environment.

References

[1] Sufian, A., Russell, A. R. "Microstructural pore changes and energy dissipation in Gosford sandstone during pre-failure loading using X-ray CT", International Journal of Rock Mechanics and Mining Sciences, 57, pp. 119–131, 2013.
https://doi.org/10.1016/j.ijrmms.2012.07.021

[2] Zabler, S., Rack, A., Manke, I., Thermann, K., Tiedemann, J., Harthill, N., Riesemeier, H. "High-resolution tomography of cracks, voids and micro-structure in greywacke and limestone", Journal of Structural Geology, 30(7), pp. 876–887, 2008.
https://doi.org/10.1016/j.jsg.2008.03.002

[3] Zhao, Y., Qin, W., Jin, A., Wu, H., Chen, Z. "Research and analysis of the impact of the pore structure on the mechanical properties and fracture mechanism of sandstone", Materials Today Communications, 38, 107753, 2024.
https://doi.org/10.1016/j.mtcomm.2023.107753

[4] Zhu, J. B., Zhou, T., Liao, Z. Y., Sun, L., Li, X. B., Chen, R. "Replication of internal defects and investigation of mechanical and fracture behaviour of rock using 3D printing and 3D numerical methods in combination with X-ray computerized tomography", International Journal of Rock Mechanics and Mining Sciences, 106, pp. 198–212, 2018.
https://doi.org/10.1016/j.ijrmms.2018.04.022

[5] Apted, M. J., Ahn, J. "Geological Repository Systems for Safe Disposal of Spent Nuclear Fuels and Radioactive Waste", Woodhead Publishing, 2017. ISBN 978-0-08-100642-9 [online] Available at: https://www.sciencedirect.com/book/edited-volume/9780081006429/geological-repository-systems-for-safe-disposal-of-spent-nuclear-fuels-and-radioactive-waste [Accessed: 01 December 2025]

[6] Bukovská, Z., Soejono, I., Vondrovic, L., Vavro, M., Souček, K., …, Veselovský, F. "Characterization and 3D visualization of underground research facility for deep geological repository experiments: A case study of underground research facility Bukov, Czech Republic", Engineering Geology, 259, 105186, 2019.
https://doi.org/10.1016/j.enggeo.2019.105186

[7] Liu, Y., Wang, P., Yang, M., Zhao, Y., Zhao, J., Song, Y. "CO_2 sequestration in depleted methane hydrate sandy reservoirs", Journal of Natural Gas Science and Engineering, 49, pp. 428–434, 2018.
https://doi.org/10.1016/j.jngse.2017.10.023

[8] Rezk, M. G., Foroozesh, J., Zivar, D., Mumtaz, M. "CO_2 storage potential during CO_2 enhanced oil recovery in sandstone reservoirs", Journal of Natural Gas Science and Engineering, 66, pp. 233–243, 2019.
https://doi.org/10.1016/j.jngse.2019.04.002

[9] Řimnáčová, D., Weishauptová, Z., Přibyl, O., Sýkorová, I., René, M. "Effect of shale properties on CH_4 and CO_2 sorption capacity in Czech Silurian shales", Journal of Natural Gas Science and Engineering, 80, 103377, 2020.
https://doi.org/10.1016/j.jngse.2020.103377

[10] Angeli, M., Bigas, J.-P., Benavente, D., Menéndez, B., Hébert, R., David, C. "Salt crystallization in pores: quantification and estimation of damage", Environmental Geology, 52(2), pp. 205–213, 2007.
https://doi.org/10.1007/s00254-006-0474-z

[11] Benavente, D., Cueto, N., Martínez-Martínez, J., García del Cura, M. A., Cañaveras, J. C. "The influence of petrophysical properties on the salt weathering of porous building rocks", Environmental Geology, 52(2), pp. 215–224, 2007.
https://doi.org/10.1007/s00254-006-0475-y

[12] Ruedrich, J., Siegesmund, S. "Salt and ice crystallisation in porous sandstones", Environmental Geology, 52(2), pp. 225–249, 2007.
https://doi.org/10.1007/s00254-006-0585-6

[13] Martinec, P., Vavro, M., Scucka, J., Maslan, M. "Properties and durability assessment of glauconitic sandstone: a case study on Zamel sandstone from the Bohemian Cretaceous Basin (Czech Republic)", Engineering Geology, 115(3–4), pp. 175–181, 2010.
https://doi.org/10.1016/j.enggeo.2009.08.005

[14] Přikryl, R., Weishauptová, Z., Novotná, M., Přikrylová, J., Šťastná, A. "Physical and mechanical properties of the repaired sandstone ashlars in the facing masonry of the Charles Bridge in Prague (Czech Republic) and an analytical study for the causes of its rapid decay", Environmental Earth Sciences, 63(7), pp. 1623–1639, 2011.
https://doi.org/10.1007/s12665-010-0819-5

[15] Vavro, M., Vavro, L., Martinec, P., Souček, K. "Properties, durability and use of glauconitic Godula sandstones: a relatively less known building stone of the Czech Republic and Poland", Environmental Earth Sciences, 75(22), 1437, 2016.
https://doi.org/10.1007/s12665-016-6248-3

[16] Rasiņa, M., Lūsēns, M., Racek, M., Přikrylová, J., Weishauptová, Z., Řimnáčová, D., Přikryl, R. "Distinction between consecutive construction phases by combined microscopic study and quantitative pore space analysis: Case study of Horn's Bastion, Riga Castle (Latvia)", Journal of Cultural Heritage, 57, pp. 88–96, 2022.
https://doi.org/10.1016/j.culher.2022.08.004

[17] Kuhlman, K. L., Matteo, E. N. "Porosity and Permeability: Literature Review and Summary", In: Proceedings of the 9th Conference on Mechanical Behavior of Salt (SaltMech IX), Hannover, Germany, 2018, pp. 15–27. ISBN 978-3-9814108-6-0 [online] Available at: https://kris.kuhlmans.net/papers/60_1476_2018-02-02_kuhlman-perm-porosity1.pdf [Accessed: 01 December 2025]

[18] Freire-Lista, D. M., Fort, R., Varas-Muriel, M. J. "Freeze–thaw fracturing in building granites", Cold Regions Science and Technology, 113, pp. 40–51, 2015.
https://doi.org/10.1016/j.coldregions.2015.01.008

[19] Jun, J., Liang, W. "Investigation of the pore structure characteristics and fluid components of Quaternary mudstone biogas reservoirs: a case study of the Qaidam Basin in China", Scientific Reports, 14(1), 26512, 2024.
https://doi.org/10.1038/s41598-024-78010-4

[20] Rübner, K., Hoffmann, D. "Characterization of Mineral Building Materials by Mercury-Intrusion Porosimetry", Particle & Particle Systems Characterization, 23(1), pp. 20–28, 2006.
https://doi.org/10.1002/ppsc.200601008

[21] Thommes, M., Kaneko, K., Neimark, A. V., Olivier, J. P., Rodriguez-Reinoso, F., Rouquerol, J., Sing, K. S. W. "Physisorption of gases, with special reference to the evaluation of surface area and pore size distribution (IUPAC Technical Report)", Pure and Applied Chemistry, 87(9–10), pp. 1051–1069, 2015.
https://doi.org/10.1515/pac-2014-1117

[22] Wang, W., Li, W., Xu, S. "Classifications of the Reservoir Space of Tight Sandstone Based on Pore Structure, Connectivity, and Fractal Character: A Case Study from the Chang 7 Member of the Triassic Yanchang Formation in the Ordos Basin, China", ACS Omega, 7(12), pp. 10627–10637, 2022.
https://doi.org/10.1021/acsomega.2c00252

[23] Zeng, S., Li, H., Zhang, N., Sun, B., Li, J., Liu, Y. "Full-scale pore size distribution features of uranium-bearing sandstone in the northwest of Xinjiang, China", Royal Society Open Science, 8(5), 202036, 2021.
https://doi.org/10.1098/rsos.202036

[24] Andrushia, D. A., Anand, N., Lublóy, É., Naser, M. Z., Kanagaraj, B. "SEM Image-based Porosity Analysis of Fire Damaged High Strength Concrete", Periodica Polytechnica Civil Engineering, 68(2), pp. 559–570, 2024.
https://doi.org/10.3311/PPci.22917

[25] Hołaj-Krzak, J. T., Dybek, B., Szymenderski, J., Koniuszy, A., Wałowski, G. "Unconventional Fossil Energy Carrier Assessment of the Influence of the Gas Permeability Coefficient on the Structure of Porous Materials: A Review", Energies, 18(4), 870, 2025.
https://doi.org/10.3390/en18040870

[26] Šperl, J., Trčková, J. "Permeability and porosity of rocks and their relationship based on laboratory testing", Acta Geodynamica et Geomaterialia, 5(1), pp. 41–47, 2008. [online] Available at: https://www2.irsm.cas.cz/materialy/acta_content/2008_01/4_Trckova.pdf [Accessed: 01 December 2025]

[27] Konečný, P., Kožušníková, A. "Characterizing gas permeability and pore properties of Czech granitic rocks", Acta Geodynamica et Geomaterialia, 13(4), pp. 331–338, 2016.
https://doi.org/10.13168/AGG.2016.0015

[28] Cnudde, V., Boone, M. N. "High-resolution X-ray computed tomography in geosciences: A review of the current technology and applications", Earth-Science Reviews, 123, pp. 1–17, 2013.
https://doi.org/10.1016/j.earscirev.2013.04.003

[29] Cnudde, V., Cwirzen, A., Masschaele, B., Jacobs, P. J. S. "Porosity and microstructure characterization of building stones and concretes", Engineering Geology, 103(3–4), pp. 76–83, 2009.
https://doi.org/10.1016/j.enggeo.2008.06.014

[30] Capek, P., Vesely, M., Svoboda, M., Remzova, M., Zouzelka, R., Kocirik, M., Brabec, L., Rathousky, J. "Bohemian sandstone for restoration of cultural heritage sites: 3D microstructure and mass transport properties", Heritage Science, 11(1), 36, 2023.
https://doi.org/10.1186/s40494-022-00854-8

[31] Košek, F., Dudák, J., Tymlová, V., Žemlička, J., Řimnáčová, D., Jehlička, J. "Evaluation of pore-fracture microstructure of gypsum rock fragments using micro-CT", Micron, 181, 103633, 2024.
https://doi.org/10.1016/j.micron.2024.103633

[32] Kovářová, K., Ševčík, R., Weishauptová, Z. "Comparison of mercury porosimetry and X-ray microtomography for porosity study of sandstones", Acta Geodynamica et Geomaterialia, 9(4), pp. 541–549, 2012. [online] Available at: https://www.irsm.cas.cz/materialy/acta_content/2012_04/11.Kovarova.pdf [Accessed: 01 December 2025]

[33] Nakashima, Y., Nakano, T., Nakamura, K., Uesugi, K., Tsuchiyama, A., Ikeda, S. "Three-dimensional diffusion of non-sorbing species in porous sandstone: computer simulation based on X-ray microtomography using synchrotron radiation", Journal of Contaminant Hydrology, 74(1–4), pp. 253–264, 2004.
https://doi.org/10.1016/j.jconhyd.2004.03.002

[34] Nakashima, Y., Watanabe, Y. "Estimate of transport properties of porous media by microfocus X-ray computed tomography and random walk simulation", Water Resources Research, 38(12), pp. 8-1–8-12, 2002.
https://doi.org/10.1029/2001WR000937

[35] Sato, A., Ikeda, K. "Visualization of diffusion phenomena in porous media by means of X-ray computed tomography (CT) scanning", Canadian Geotechnical Journal, 52(10), pp. 1448–1456, 2015.
https://doi.org/10.1139/cgj-2014-0451

[36] Sato, A., Obara, Y. "Analysis of Pore Structure and Water Permeation Property of a Shale Rock by Means of X-Ray CT", Procedia Engineering, 191, pp. 666–673, 2017.
https://doi.org/10.1016/j.proeng.2017.05.230

[37] Kotlík, P., Heidingsfeld, V., Vaneček, J., Bayer, K., Kaše, J., Váňa, J., Weber, J. "The rescue of M. Braun's sculptures in the area of Betlém near Kuks (CZ): a case study of sandstone deterioration in the frame of an international project", In: Proceedings of the 8th International Congress on Deterioration and Conservation of Stone, Berlin, Germany, 1996, pp. 955–967. ISBN 3000007792

[38] Rybařík, V. "Ušlechtilé stavební a sochařské kameny České republiky" (Noble building and sculptural stone of the Czech Republic), Industrial Secondary School of Stonework and Sculpture in Hořice, 1994. ISBN 80-900041-5-6 (in Czech)

[39] Toesca, M. "Thermo-Mechanical Analysis of Charles Bridge in Prague", MSc Thesis, Czech Technical University in Prague, 2014.

[40] Laboratory Imaging s.r.o. "NIS-ELEMENTS (5.30.00)", [computer program] Laboratory Imaging s.r.o., Praha, Czech Republic, 2020.

[41] Rigaku Corporation "PDXL 2 (2.4.2.0)", [computer program] Rigaku Corporation, Tokyo, Japan, 2018.

[42] International Centre for Diffraction Data "PDF-2 2015", [database] International Centre for Diffraction Data, Newtown Square, PA, USA, 2015.

[43] ČSN "ČSN 72 1155 Stanovení nasákavosti a zdánlivé pórovitosti přírodního stavebního kamene" (ČSN 72 1155 Determination of water absorption and apparent porosity of natural building stone), Office for Standards and Testing, Praha, Czech Republic, 1984. (in Czech)

[44] Vavro, M., Vavro, L., Kubina, L. "Gas permeability of rocks and its use for monitoring crack propagation during compressive strength testing", In: Proceedings of the ISRM International Symposium EUROCK 2025, Trondheim, Norway, 2025, pp. 1–7. ISBN 978-82-8208-079-8 [online] Availble at: https://airdrive.eventsair.com/eventsairwesteuprod/production-atlanticmice-public/66d0368f-d7e74c0684a9e53cafa78f4f [Accessed: 01 December 2025]

[45] Volume Graphic GmbH "VGStudio MAX (3.3.2)", [computer program] Volume Graphic GmbH, Heidelberg, Germany, 2019.

[46] Wentworth, C. K. "A Scale of Grade and Class Terms of Clastic Sediments", The Journal of Geology, 30(5), pp. 377–392, 1922. [online] Available at: https://www.jstor.org/stable/30063207 [Accessed: 01 December 2025]

[47] IUPAC "Manual of Symbols and Terminology for Physicochemical Quantities and Units - Appendix II. Definitions, Terminology and Symbols in Colloid and Surface Chemistry. Part II: Heterogeneous Catalysis", Pure and Applied Chemistry, 46(1), pp. 71–90, 1976.
https://doi.org/10.1351/pac197646010071

[48] Koutník, P., Antoš, P., Hájková, P., Martinec, P., Antošová, B., Ryšánek, P., Pacina, J., Šancer, J., Ščučka, J., Brůna, V. "Decorative stones of Bohemia, Moravia and Czech Silesia", Jan Evangelista Purkyně University in Ústí nad Labem, 2015. ISBN 978-80-7414-974-0 [online] Available at: http://kamenolomy.fzp.ujep.cz/eng/index.php?page=project [Accessed: 01 December 2025]

[49] Singhal, B. B. S., Gupta, R. P. "Applied Hydrogeology of Fractured Rocks", Springer Dordrecht, 2010. ISBN 978-90-481-8798-0
https://doi.org/10.1007/978-90-481-8799-7

[50] Kočí, V., Maděra, J., Fořt, J., Žumár, J., Pavlíková, M., Pavlík, Z., Černý, R. "Service Life Assessment of Historical Building Envelopes Constructed Using Different Types of Sandstone: A Computational Analysis Based on Experimental Input Data", The Scientific World Journal, 2014(1), 802509, 2014.
https://doi.org/10.1155/2014/802509

[51] Kytýř, D., Koudelka, P., Drozdenko, D., Vavro, M., Fíla, T., Rada, V., Vavro, L., Máthis, K., Souček, K. "Acoustic emission and 4D X-ray micro-tomography for monitoring crack propagation in rocks", International Journal of Rock Mechanics and Mining Sciences, 183, 105917, 2024.
https://doi.org/10.1016/j.ijrmms.2024.105917

[52] Vavrik, D., Benes, P., Fila, T., Koudelka, P., Kumpova, I., Kytyr, D., Vopalensky, M., Vavro, M., Vavro, L. "Local fracture toughness testing of sandstone based on X-ray tomographic reconstruction", International Journal of Rock Mechanics and Mining Sciences, 138, 104578, 2021.
https://doi.org/10.1016/j.ijrmms.2020.104578

[53] Goupil, M., Heap, M. J., Baud, P. "Permeability anisotropy in sandstones from the Soultz-sous-Forêts geothermal reservoir (France): implications for large-scale fluid flow modelling", Geothermal Energy, 10(1), 32, 2022.
https://doi.org/10.1186/s40517-022-00243-1

[54] Fauzi, U., Hoerdt, A., Neubauer, F. M. "Influence of coordination number and percolation probability on rock permeability estimation", Geophysical Research Letters, 29(8), pp. 78-1–78-4, 2002.
https://doi.org/10.1029/2001GL013414